Robotica (1998) volume 16, pp. 75–87. Printed in the United Kingdom © 1998 Cambridge University Press

High-bandwidth force and impedance control for industrial robots

Eckhard Freund and Jürgen Pesara

Institute of Robotics Research, University of Dortmund, D-44227 Dortmund (Germany)
email: freund@damon.irf.uni-dortmund.de or pesara@damon.irf.uni-dortmund.de

(Received in final form: April 9, 1997)

SUMMARY

Common geared industrial robots call for force control methods with special properties such as good rejection of frictional disturbances, smoothness of corrective motions, and more. A new method is presented which meets these requirements and provides a high control bandwidth. In the manner of hybrid control, directions of a task frame can be selected to be force, impedance or position controlled. A joint-based inner position loop and a superimposed predictive force controller are used. Practical results include data from a robotic grinding facility. Here, the controller proved robustness and good performance under rough conditions.

KEYWORDS: Industrial robots; Force control; Impedance control; Predictive control; Inner loop.

1 INTRODUCTION

Many processing or assembly tasks require the control of contact forces rather than pure positon control. Position control is sufficient only in case of exactly positioned workpieces of well-known shape, a robot of high positioning accuracy and perfect tools. In practical applications it often is impossible or uneconomic to satisfy these conditions. A force controlled robot in contrast can cope with uncertainties, tolerances, detrition of tools etc.

The contact forces can be measured with a force-torque sensor that is mounted in the robot's wrist. Methods to feedback the force measurements have been developed by many researchers. A survey of the early ones is given by Whitney.[1] The methods can roughly be divided into *explicit force control* which aims at tracking a commanded set point of force and into *impedance control* which makes the robot respond to contact forces like an artificial system of mass, spring and damper. Generally, a *task frame* can be specified of which some directions are force controlled and others are position controlled.[2] This is referred to as *hybrid control*[3] and can be extended by replacing position control with impedance control.[4]

In spite of the big effort in research over the past decades, there is still only negligible application of force control in industrial environments. One reason for this – among several others – is the fact that many force control methods simply cannot be applied to real industrial robots, and with all known methods the achievable force control bandwidth is too slow for many applications. The problems with industrial robots (in contrast to some experimental robots) are caused by friction and flexibilities which mainly are due to their gears. This requires a force controller with good rejection of frictional disturbances and smooth corrective motions in order not to excite vibrations.

In this paper a new force control method is presented which is very well applicable to industrial robots and provides high bandwidth. It allows both explicit force control and inpedance control. Distance control is possible, too.

2 FORCE FEEDBACK STRUCTURES

In the past, many force feedback structures have been developed. They can be classified into methods that directly supply the driving torques (called *direct* or *torque based* methods) and those methods that use an underlying position control loop (called *inner loop* or *position based* methods). In addition, there exists a minor group of methods with an underlying velocity control loop. This criterion of classification has been used in previous surveys.[5,6] Most classical force control methods such as Raibert and Craig's *hybrid position/force control,*[3] Shin and Lee's *resolved-acceleration force control*[7] and Khatib's *operational space force control*[8] are torque based. Position based methods have been introduced by Hirzinger and Landzettel,[9] Maples and Becker,[5] and De Schutter and Van Brussel.[10]

There are some important advantages of the inner loop approach over the torque based and velocity based methods which in part have been reported by Maples and Becker:[5]

- The controllers of industrial robots do not provide an interface to the driving torques, so they have to be replaced by special experimental controllers in order to implement a torque-based force control method. However, the controllers of industrial robots are equipped with a well-tuned position feedback loop and many controllers provide an interface to the set point of position which can be used for force control.
- Industrial robots often require different adjustments for their joint-based position controllers to cope with different joint characteristics concerning flexibilities and Coulomb friction. Cartesian position control schemes which are the basis of direct force control methods are inadequate in this case.

https://doi.org/10.1017/S0263574798000162 Published online by Cambridge University Press

- The computationally expensive force feedback loop can be implemented with a slower rate than the inner position loop. The position loop (and the force loop of direct methods) must be very fast in order to stabilize the natural oscillations of the industrial robot's joints which are due to their flexibilities.
- The most important advantage of the inner-loop approach is its ability to realize a high-gain position feedback loop and a slower external force feedback loop. The high-gain position feedback is necessary to achieve a good rejection of Coulomb friction and other disturbances acting in industrial robots. This can only be realized with a fast position sensor. The loop closure with a force sensor cannot provide high gain because of its dead time and low-pass dynamics. Thus, direct force control methods show poor disturbance rejection. Some disturbance effects of the nonlinear robot dynamics can be compensated by an inverse model which therefore has been inserted into most direct methods. But at least Coulomb friction – which in practice is time-varying and position dependent – cannot be compensated completely. For this reason, direct force control methods mostly have been realized with experimental robots equipped with low-friction direct drives only. In contrast to this, inner loop methods have been realized successfully with industrial robots.

The basic idea of the inner loop approach is to transform the force deviation into a desired change of position

$$\Delta p_{des} = \frac{f_{des} - f_{act}}{k_s}. \qquad (1)$$

In equation (1) f_{des} and f_{act} are the desired and actual force, and k_s is an assumed stiffness constant. With this approach distance control can be achieved very easily by replacing the force values with distance values, and replacing the stiffness constant with -1.

In order to achieve a change of position the external force controller supplies positional increments in task space ${}^{task}\delta\mathbf{p}$. This six-dimensional vector contains increments of both translation and rotation. The increments have to be added up, superimposed on the planned trajectory, and passed to the joint-space position servo. There is a variety of ways to arrange the necessary summations and coordinate transformations.

One possibility is to transform the task-space increments ${}^{task}\delta\mathbf{p}$ into joint increments $\delta\mathbf{q}$ and to add up these.[10] This is shown in Figure 1. The transformation is performed in sequential steps with intermediate data in tool and in base coordinates. The increments are transformed into another Cartesian coordinate system by multiplying both the translational and the rotational part with an orientation matrix $\mathbf{R}$. The subsequent transformation from base coordinates into joint space is performed by multiplication with the inverse jacobian $\mathbf{J}^{-1}$ or an equivalent transformation of velocity. The summation and the computation of associated velocity and acceleration (which are necessary to enable feedforward) are expressed by discrete transfer functions (z-transforms). The corrective motion $\mathbf{q}_{cor}$ is then superimposed on the planned trajectory $\mathbf{q}_{pln}$ yielding the set point of position for the joint-space position servo $\mathbf{q}_{des}$.

Alternatively to this control signal interface, the summation can be performed in base coordinates[5] or in tool coordinates.[9] The Cartesian summation requires more computation than the joint-space summation but it is advantageous in case of redundant robots. Moreover, some industrial robot controllers provide Cartesian interface for path corrections.

For all these multi-dimensional control signal interfaces the feedback dynamics can be modeled by independent one-dimensional loops for each coordinate of the task space. This is depicted in Figure 2 where p_{pln} is the planned trajectory, p_{cor} is its correction, p_{des} is the resulting corrected set point of position, p_{act} is the actual position, and p_{env} is the position of the environment which acts as disturbance.

The summing unit in Figure 2 represents the control signal interface. For continuous controller design, it can

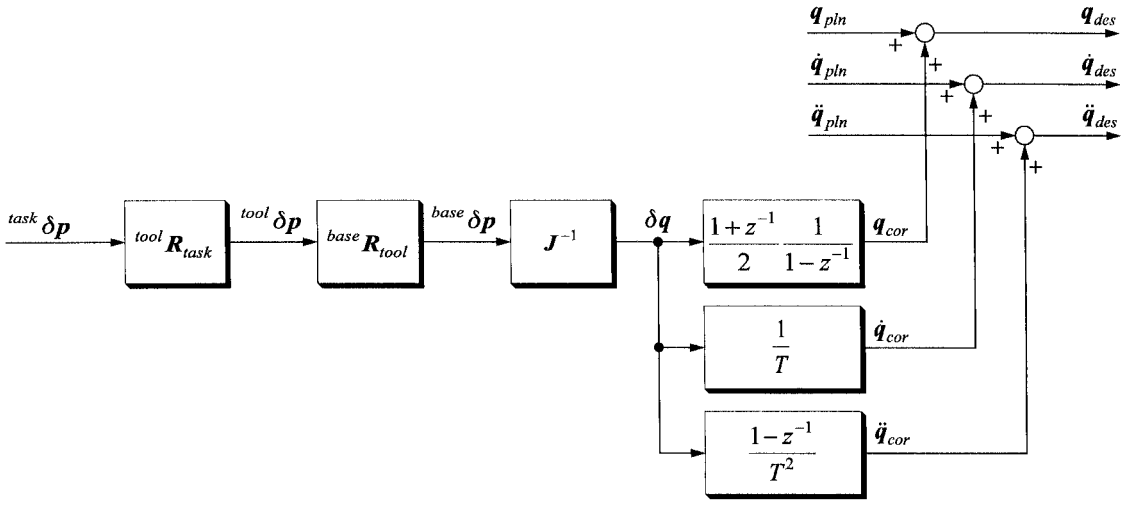

Fig. 1. Control signal interface with summation in joint space.

https://doi.org/10.1017/S0263574798000162 Published online by Cambridge University Press

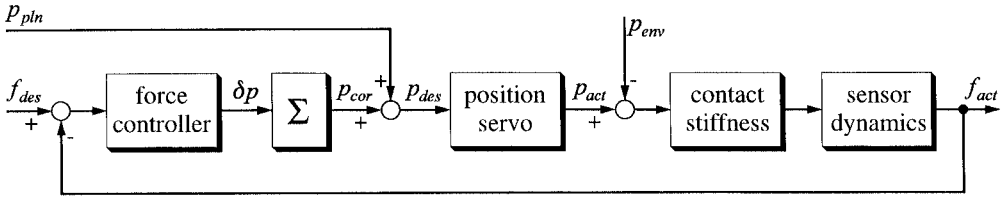

Fig. 2. One-dimensional force feedback loop.

be modeled by an integrator. In digital implementations, the summation of the positional increments δp and the computation of feedforward terms is performed according to the discrete transfer functions given in Figure 1:

$$p_{cor,k} = p_{cor,k-1} + \tfrac{1}{2}(\delta p_k + \delta p_{k-1}), \tag{2}$$

$$\dot{p}_{cor,k} = \frac{1}{T}\delta p_k, \tag{3}$$

$$\ddot{p}_{cor,k} = \frac{1}{T^2}(\delta p_k - \delta p_{k-1}), \tag{4}$$

where T is the sampling interval and k is its count.

The position loop dynamics can be modeled by a second-order system:

$$G_r(s) = \frac{\omega_r^2}{s^2 + 2\zeta_r\omega_r s + \omega_r^2}. \tag{5}$$

This model will be used for simulations throughout this paper. Following De Schutter and Van Brussel,[10] a damping ratio $\zeta_r = 0.75$ is chosen. A frequency $\omega_r = 50\,\mathrm{s}^{-1}$ is assumed exemplarily.

The sensor dynamics which results from filtering and communication delay can be modeled by a first-order system plus dead time:

$$G_s(s) = \frac{a_s}{s + a_s} e^{-s\tau_s}. \tag{6}$$

In simulations the sensor dynamics will be neglected for simplicity. In practical applications equation (6) will be included to enable high-bandwidth control.

The simplest model of contact stiffness is a single constant k_s as implied by equation (1). More generally, inertia and damping terms could be considered. For subsequent simulations a stiffness of $k_s = 1000\,\mathrm{N/m}$ is assumed.

The structure depicted in Figure 2 works for explicit force control as well as for impedance control. In the following, explicit force control is considered first. An extension towards impedance control is given subsequently.

3 REQUIREMENTS AND KNOWN FORCE CONTROLLERS

The external force controller shall meet the following requirements in order to be suitable for practical application:

- no steady-state error,
- no overshooting,
- high bandwidth,
- smoothness, i.e. the correction of position shall be differentiable in order not to excite vibrations,
- robustness with respect to varying position loop dynamics and inexactly known stiffness constant,
- little on-line computation,
- easily adjustable controller parameters.

In the literature, mostly PID type controllers and similar have been applied. Volpe and Khosla[11] give a survey of these and state the proportional controller to be best (they as well as some other authors call it integral controller because they consider the integrator from the control signal interface as part of the controller). However, the proportional controller generates continuous but not differentiable corrections of position. A first-order low-pass filter gives differentiability but it decreases the achievable bandwidth. All these controllers overshoot, the higher the bandwidth is adjusted. Simulation results for a step of 1 N in f_{des} with $p_{\mathrm{pln}} = 0$ are shown in Figure 3. According to De Schutter and Van Brussel,[10] the controller adjustments are $k_P = 0.5\omega_r/k_s$ for the proportional controller, and $k_P = \omega_r/k_s$, $k_D = 1/k_s$ for the proportional-plus-derivative controller. The low-pass controller's pole is placed at $s = -50\,\mathrm{s}^{-1}$, and its proportional gain is adjusted to $k_P = 0.32\omega_r/k_s$ so that it produces the same overshoot is as the proportional controller.

Many other controller types have been investigated by various researchers, including state-space feedback,[12] adaptive strategies,[13] neural networks,[14] and fuzzy control.[15] However, none of these meets all the requirements. The most common deficiencies are unsmoothed corrections and a low closed-loop bandwidth.

4 A NEW APPROACH

The basic idea is to create a new desired position p^*_{des} which shall be tracked by the set point of position p_{des} with configurable dynamics. The desired position p^*_{des} is the actual position plus the desired change given in equation (1). Since the actual position is not known within the force controller, an estimate $\hat{p}^*_{act}$ is used:

$$p^*_{des} = \hat{p}^*_{act} + \Delta p_{des}. \tag{7}$$

The estimate is computed by a plant model which covers the integrator from the control signal interface, the position servo, and the sensor dynamics. The resulting control structure is depicted in Figure 4. Here already a simple low-pass filter is included which lets the set-point

https://doi.org/10.1017/S0263574798000162 Published online by Cambridge University Press

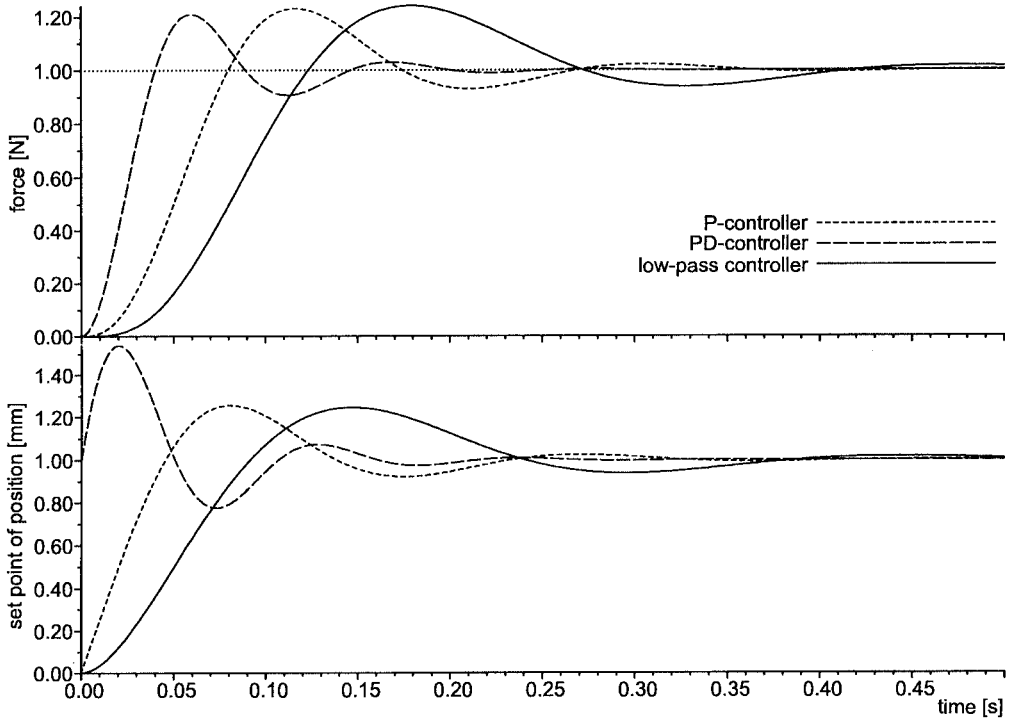

Fig. 3. Simulated step responses of simple force controllers.

estimate $\hat{p}_{des}$ track p^*_{des}. The real set point p_{des} follows with an offset caused by p_{pln}. The low-pass filter makes use of the integrator which is part of the plant model. With this and the P-unit c a first-order system with a pole at $s = -c$ results. Figure 5 shows a simulated step response of this controller with $c = 50\,\mathrm{s}^{-1}$. For comparison the response of the proportional controller from Figure 3 is given. In contrast to this one, the set point of position p_{des} does not overshoot. Instead, it shows the response of a first-order system. The actual force value follows with the dynamics given by the position servo and the sensor. It overshoots slightly because of $\zeta_r < 1$ in equation (5).

The control structure is similar to a Smith predictor which has been developed for systems with dead time.[16] Its general structure is depicted in Figure 6. The plant function consists of two parts:

$$G_P(s) = G_1(s)G_2(s) \quad \text{with} \quad G_2(s) = e^{-s\tau}. \tag{8}$$

The Smith predictor uses a plant model

$$\hat{G}_P(s) = \hat{G}_1(s)\hat{G}_2(s). \tag{9}$$

If the model is correct, a simplified structure results where the dead time is removed from the feedback loop, as shown in Figure 6. Thus standard techniques can be applied to design the internal controller $G'_R(s)$.

This concept works for all stable dynamics with a steady-state gain of 1 as $G_2(s)$ and can be applied to the force control problem with

$$G_1(s) = \frac{k_s}{s}, \tag{10}$$

$$G_2(s) = G_r(s)G_s(s). \tag{11}$$

Stabilization of $G_1(s)$ is achieved with a simple proportional controller

$$G'_R(s) = \frac{c}{k_s} \tag{12}$$

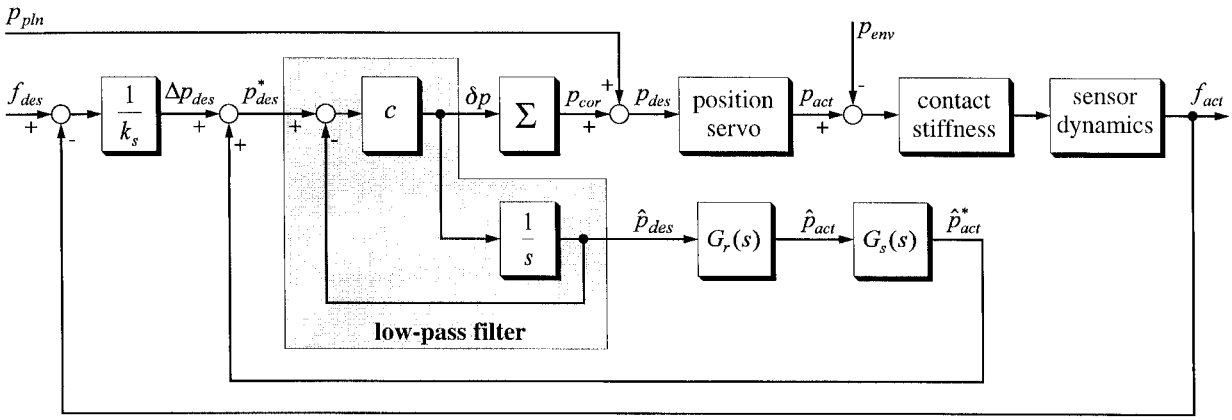

Fig. 4. New model based control structure.

https://doi.org/10.1017/S0263574798000162 Published online by Cambridge University Press

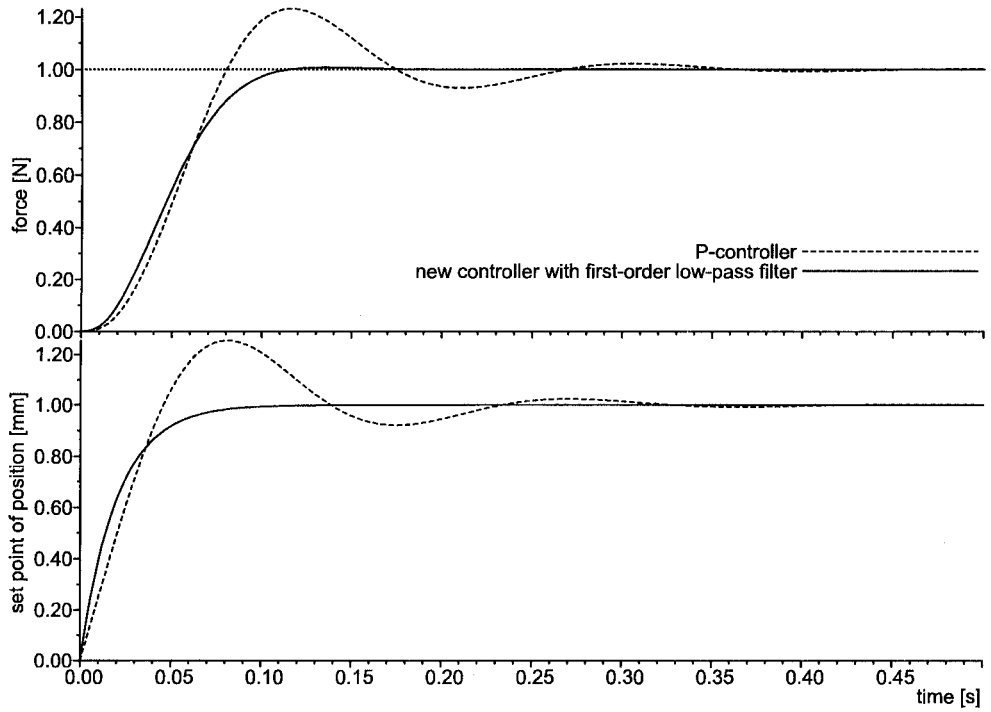

Fig. 5. Simulated step response of new controller.

which leads to a first-order system as closed-loop dynamics for the inner part. According to Figure 6, the complete dynamics of the closed force feedback loop is given by the dynamics resulting from the inner feedback of $G_1(s)$ multiplied with the second part of the plant dynamics:

$$G_f(s) = \frac{f_{act}}{f_{des}} = \frac{c}{s+c} G_r(s) G_s(s). \tag{13}$$

The resulting feedback structure becomes equal to that one depicted in Figure 4 if the stiffness constant is shifted so that positions instead of forces are predicted. Thus, the new force feedback structure can be regarded as a modified Smith predictor. It follows that the controller performs well for dynamics with long dead time, too.

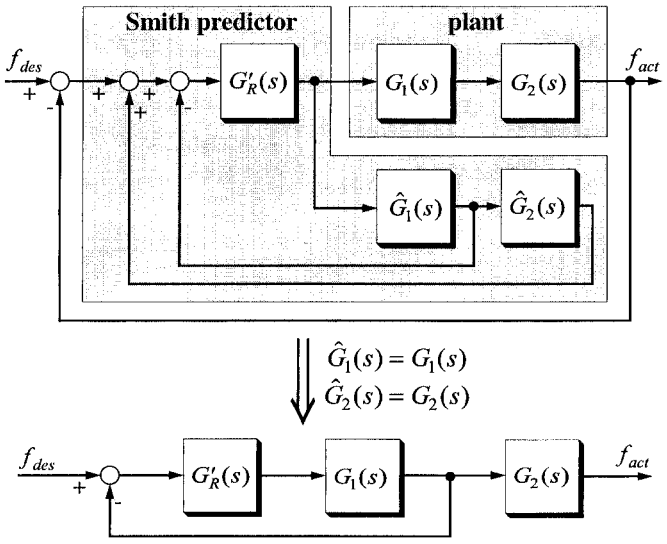

Fig. 6. Smith predictor.

5 SMOOTHING THE CORRECTIONS

As can be seen in Figure 5, the new controller so far produces non-differentiable corrections of the position. Therefore the first-order low-pass filter is replaced by a second-order one. This is done with a proper design of the controller G'_R for the first part of the plant model, an integrator here. A computationally efficient structure is obtained with a state-space design for an artificial plant with an additional integrator in front. Taking into account the discrete summation from equation (2) and choosing the state variables $x_1 = \delta p$ and $x_2 = p_{cor}$, the state-space model of the artificial plant is

$$\begin{bmatrix} x_{1,k+1} \\ x_{2,k+1} \end{bmatrix} = \begin{bmatrix} 1 & 0 \\ 1 & 1 \end{bmatrix} \begin{bmatrix} x_{1,k} \\ x_{2,k} \end{bmatrix} + \begin{bmatrix} 1 \\ \frac{1}{2} \end{bmatrix} u. \tag{14}$$

The model imput u is the increment of δp and thus proportional to the acceleration; see equation (4). It is connected to the output of a state-space controller with p^*_{des} as desired value:

$$u = v p^*_{\mathrm{des}} - k_1 x_1 - k_2 x_2. \tag{15}$$

The feedback gains can be determined by pole-placement using Ackermann's formula. A placement of both poles at $z = e^{-cT}$ yields the vector of feedback gains

$$\begin{bmatrix} k_1 \\ k_2 \end{bmatrix} = \begin{bmatrix} \frac{3}{2} - e^{-cT} - \frac{1}{2} e^{-2cT} \\ 1 - 2e^{-cT} + e^{-2cT} \end{bmatrix}. \tag{16}$$

For steady-state accuracy the gain of the prefilter v must

https://doi.org/10.1017/S0263574798000162 Published online by Cambridge University Press

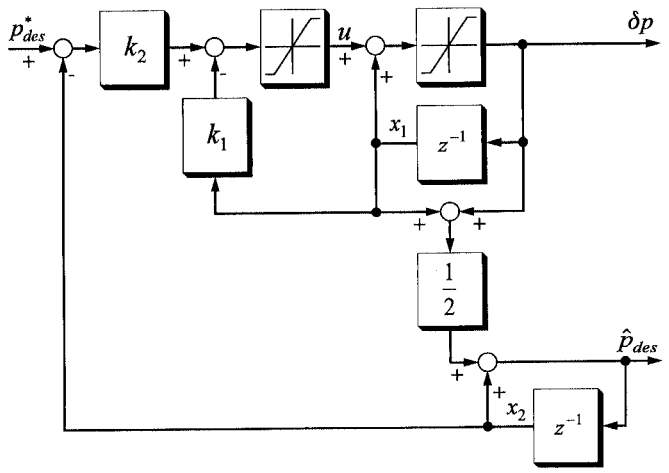

Fig. 7. Second-order low-pass filter with limiters for velocity and acceleration.

be equal to k_2 which simplifies the low-pass filter's structure as depicted in Figure 7. If this one is inserted into the control structure depicted in Figure 4, the resulting closed-loop dynamics (see equation (13)) can be described with the discrete transfer function

$$G_f(z) = \left(\frac{1 - e^{-cT}}{1 - e^{-cT}z^{-1}}\right)^2 \frac{1 + z^{-1}}{2} G_r(z)G_s(z). \quad (17)$$

Herein, the first factor is a second-order low-pass filter, the second is a transversal filter resulting from the summation according to equation (2), and the third is the unchanged dynamics of position servo and sensor.

Limitation of the corrective velocity and acceleration is an important aspect for practical application because every industrial robot has such limitations which might be exceeded by high-bandwidth corrections. The filter depicted in Figure 7 already includes appropriate limiters. The relations of the limited values δp and u to velocity and acceleration are given in equation (3) and (4), respectively.

While the limitation of velocity is unproblematic, the limitation of acceleration may result in instability if it cuts the deceleration that is demanded by the linear controller when approaching the set point. This can be avoided if the limitation of velocity is adapted properly as shown in the following.

The maximum deceleration $a_{\max}$ that occurs in the unlimited system during the stopping phase depends on the maximum velocity $v_{\max}$. It is obtained by solving the system's equation of motion for an initial velocity of $x_1(0) = v_{\max}$ and a stopping distance that can be computed from the condition $u(0) = 0$. The result can be solved for $v_{\max}$ which finally leads to

$$v_{\max} = e\frac{a_{\max}}{c}. \quad (18)$$

Figure 8 shows a simulated response to a step in f_{des} for $a_{\max} = 0.1\ \mathrm{m/s^2}$ and the response in case of no limitation. In both cases the double-pole was placed with $c = 50\ \mathrm{s}^{-1}$.

This force controller smoothes desired and measured forces simultaneously. Alternatively, separate filters could be used. Moreover, instead of a low-pass fllter path planning methods could be applied which directly allow for limitation of velocity and acceleration. However, they do not filter noisy force measurements. The method presented here provides both filtering and limitation, and is computationally very efficient.

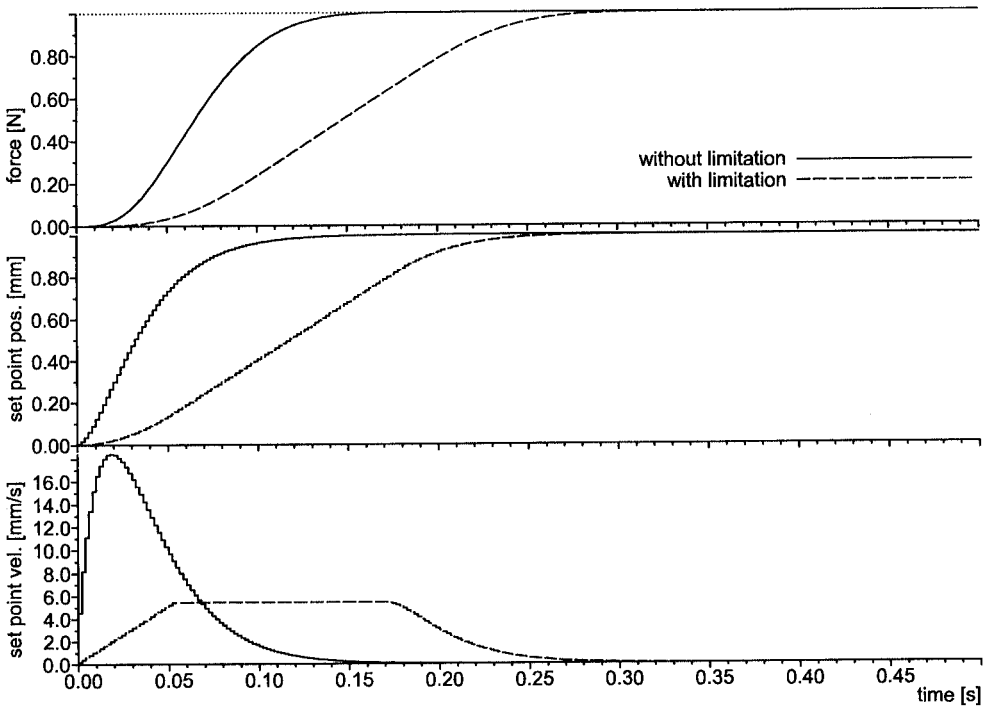

Fig. 8. Step response with second-order low-pass filter.

https://doi.org/10.1017/S0263574798000162 Published online by Cambridge University Press

6 ROBUSTNESS

Smith predictors are reputed to be of poor robustness. This is due to the circumstance that it is possible to set up a high-bandwidth feedback loop despite of the presence of a long dead time (or similar dalay as shown in this paper). In fact, robustness increases the more the bandwidth of the feedback loop is decreased.

In a comparative study the new predictive force controller with reduced bandwidth competed against some simple force controllers. The amount of overshoot and the transition to instability in case of slower dynamics or stiffer contact than modeled were investigated. The new controller performed even slightly better than the simple controllers. For example, Figure 9 shows the nominal step responses of the new controller with $c = 20\,\mathrm{s}^{-1}$ in comparison to the low-pass controller from section 3 with a pole at $s = -50\,\mathrm{s}^{-1}$ and a reduced proportional gain $k_P = 0.16\omega_r/k_s$. With this adjustment the low-pass controller overshoots less and its response is comparable to the new controller. The effect of a slower dynamics than modeled can be seen in Figure 10. The amount of overshoot is smaller for the new controller. Increasing the stiffness yields a similar behavior as can be seen in Figure 11. Again the new controller overshoots less. This is mainly due to its overshoot-free response in the case of no model error. The increase of overshoot is similar for all controllers and essentially depends on the control bandwidth.

If dynamics and contact stiffness are known imprecisely or if they vary, the bandwidth has to be reduced in order to achieve stable behavior for all variations. Moreover, the predictor's model should assume rather slow dynamics and stiff contact. This way the controller responses weakly on the average, but undesirable overshooting is avoided.

7 FEEDBACK OF THE POSITION LOOP ERROR

Whereas the sensor dynamics is invariant and therefore well predictable, the dynamics of the position loop varies because of several mechanisms:

- The nonlinear robot dynamics yields position and velocity dependent dynamics if not compensated appropriately.
- Different adjustments of the joint-space position controllers (which is typical for industrial robots) yield position-dependent dynamics in task space.
- Coulomb friction in interaction with the position controller's integral action yields slower dynamics for small deviations.

These effects are not modeled in Equation (5), and they are too complicated to be reproduced in real-time by a more sophisticated model. However, these effects spoil the prediction and thus a low-bandwidth (i.e. robust) controller has to be chosen. In particular Coulomb friction and stick-slip effects result in undesirable limit cycles if a high bandwidth is adjusted. To overcome this problem, a surprisingly simple method has been developed which is presented in the following.

The predictor contains the equation

$$\hat{p}_{act} = G_r(z)\hat{p}_{des} \tag{19}$$

to model the position feedback loop. If the position loop error $\Delta p = p_{des} - p_{act}$ is available within the force controller then equation (19) can be replaced with

$$\hat{p}_{act} = \hat{p}_{des} - \Delta p. \tag{20}$$

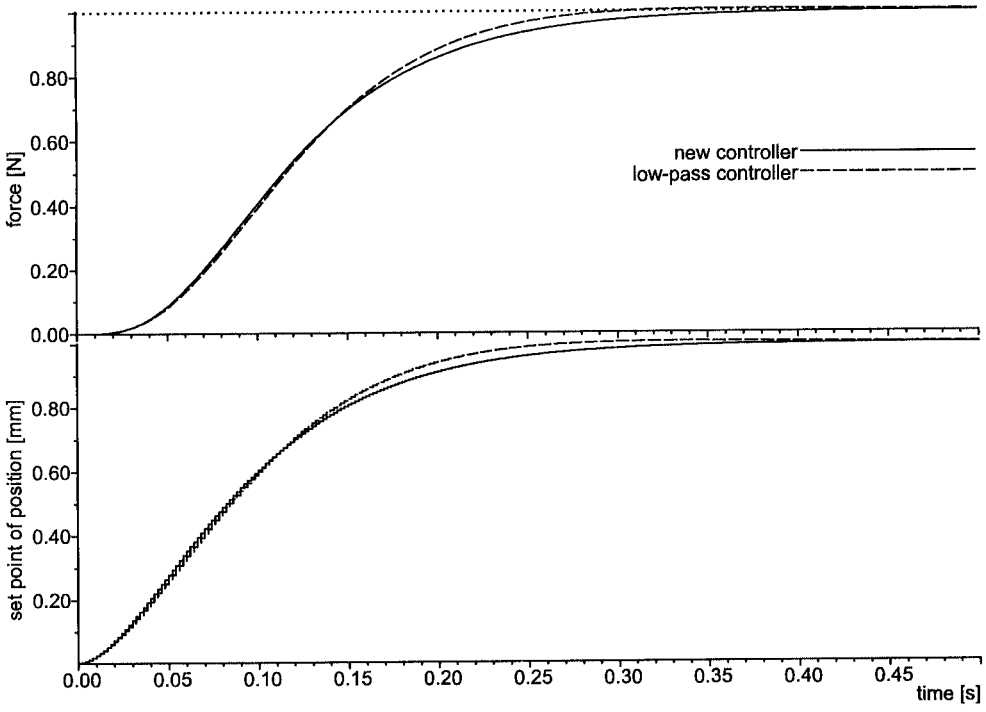

Fig. 9. New predictive controller with reduced bandwidth in comparison to low-pass controller. No model error.

https://doi.org/10.1017/S0263574798000162 Published online by Cambridge University Press

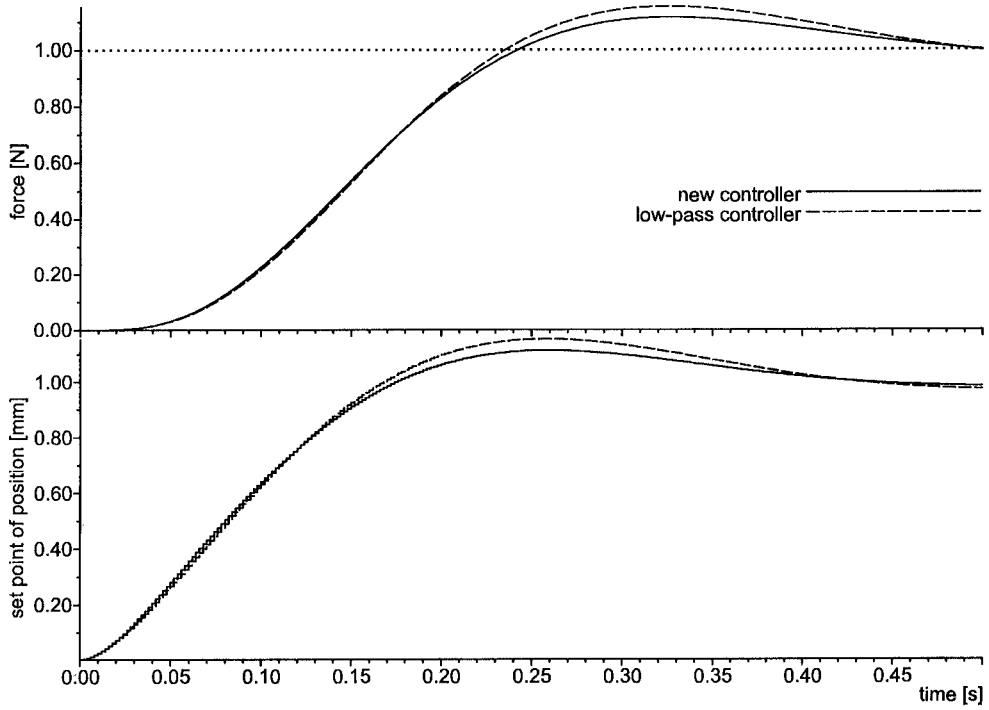

Fig. 10. Same as Figure 9, but the position servo's ω_r is $25\,s^{-1}$ instead of $50\,s^{-1}$ as modeled.

The position loop operates in joint space, thus a transformation of the joint error into task space by means of the jacobian is necessary. Since a kinematic transformation is already computed for the control signal interface, the additional amount of computation is small, especially if taking into account that the model $G_r(z)$ can be dropped.

With this perfect "prediction" all the above mentioned robustness problems with regard to the varying position loop dynamics are solved, and a high-bandwidth force control is enabled.

8 EXTENSION TO IMPEDANCE CONTROL

The objective of impedance control is to make the robot respond to environmental contact forces f_{env} with a compliant movement p_{act} that can be described by an

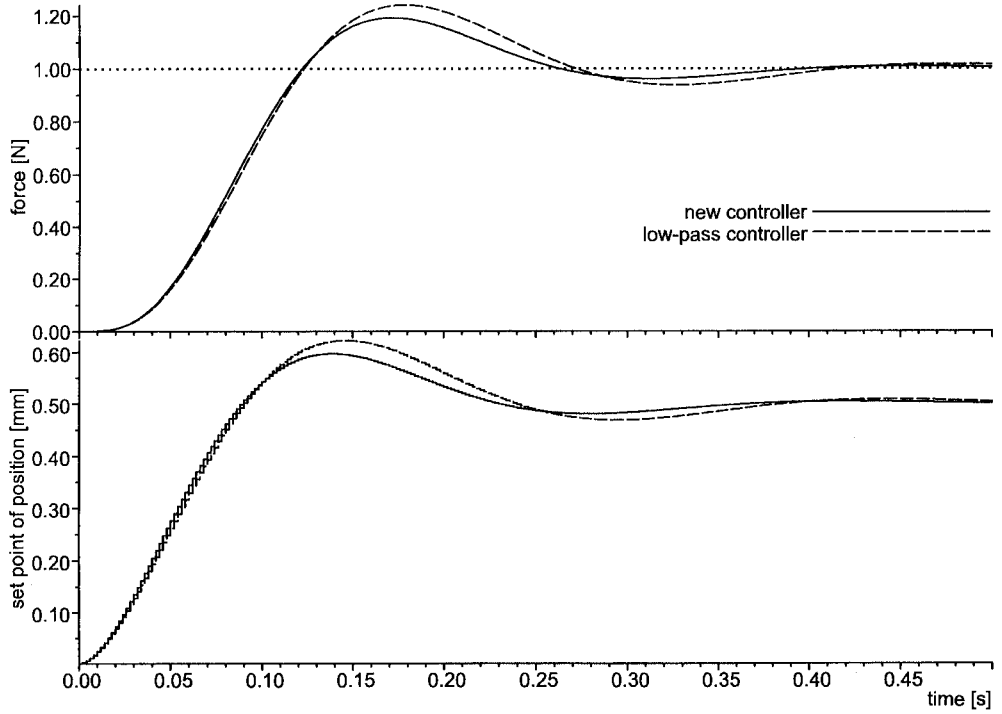

Fig. 11. Same as Figure 9, but stiffness is $k_s = 2000\,N/m$ instead of $1000\,N/m$ as modeled.

https://doi.org/10.1017/S0263574798000162 Published online by Cambridge University Press

adjustable *impedance* which usually consists of stiffness k_r, damping b_r and inertia m_r:

$$\frac{f_{env}}{p_{act}} = m_r s^2 + b_r s + k_r. \tag{21}$$

The most straightforward solution to achieve this behavior with the inner loop approach is to use an external force controller that generates positional set points from the measured force with a dynamics equal to the inverse impedance. The resulting impedance differs from the desired impedance due to the dynamics of position servo and sensor. This affects the stability when in contact and forbids arbitrary small stiffness and damping.[17] Since the force controller's output is not a position but a positional increment, the realization of this basic idea shown in Figure 12 uses an extra integrator in front of the stiffness term k_r and a feedback. The feedback loop together with the integrator from the control signal interface gives the inverse impedance. The desired value of force f_{des} acts as a bias which is zero in pure impedance control. The measured force f_{act} is the counterforce to f_{env}.

Obviously, for $k_r = 0$ this impedance controller becomes equal to an explicit force controller with a first-order low-pass filter as the transfer function. The stiffness term generates a force that pulls the robot back to the planned position.

This concept of impedance control implementation can be combined with the new force controller. Its predictor already contains the sum of positional increments in the state variable x_2 from Figure 7. It is convenient to shift the feedback with k_r so that it is located within the low-pass filter. For this a relative stiffness k_r' is defined:

$$k_r = k_r' k_s. \tag{22}$$

The new controller's extended structure is shown in Figure 13. With $k_r' = 0$ it performs explicit force control, with $k_r' > 0$ it is an impedance controller.

In contact with an environment of stiffness k_s, the simple impedance controller from Figure 12 yields a force response to a change of environmental position

$$\frac{f_{env}}{p_{env}} = k_s\left(1 - \frac{k_s G_r(s) G_s(s)}{k_s G_r(s) G_s(s) + (m_r s^2 + b_r s + k_r)}\right) \tag{23}$$

whereas the continuous-time equivalent of the new impedance controller (which is regarded for simplicity here) yields

$$\frac{f_{env}}{p_{env}} = k_s\left(1 - \frac{k_2 G_r(s) G_s(s)}{s^2 + k_1 s + k_2(1 + k_r')}\right). \tag{24}$$

In equation (23) the dynamics of position servo and sensor appear in the denominator. This causes the simple impedance controller's stability problems. In contrast to this, these delays appear only in the numerator of equation (24) where they cause no stability problems.

In order to determine the controller parameters, first an appropriate relative stiffness k_r' is chosen. Then k_1 and k_2 can be determined by pole-placement. Since the controller is realized digitally, this should be done with the discrete-time formulation of equation (24). For a double-pole at $z = e^{-cT}$ the result is equal to the vector of feedback gains given in equation (16) except that k_2 is divided by $1 + k_r'$. With these gains the response is

$$\frac{f_{env}}{p_{env}} = k_s\left(1 - \frac{1}{1 + k_r'} G_f(z)\right) \tag{25}$$

where the dynamics $G_f(z)$ is given by equation (17). The response to a step in p_{env} of 1 mm is shown in Figure 14. A stiffness $k_r = k_s$ i.e. $k_r' = 1$ has been chosen which results in a movement of 0.5 mm. The new impedance controller is parameterized with $c = 50\,\mathrm{s}^{-1}$. The simple impedance controller is parameterized so that the explicit force controller which would result for $k_r = 0$ is a first-order system with a pole at $c = 50\,\mathrm{s}^{-1}$ and a gain of $k_P = 0.32\omega_r/k_s$, see section 3. The related impedance parameters are $b_r = 1/k_P$ and $m_r = 1/ck_P$.

9 ASPECTS OF HYBRID CONTROL

Each coordinate of the task frame is controlled individually. Various controllers are possible for this. Beyond explicit force control, impedance control and (explicit) distance control which have been described so far, two further ones are useful: position control and velocity control.

From the external controller's point of view, position control essentially is a "halt" control because the planned trajectory is not corrected. The halt control can be regarded as a special case of velocity control, in which

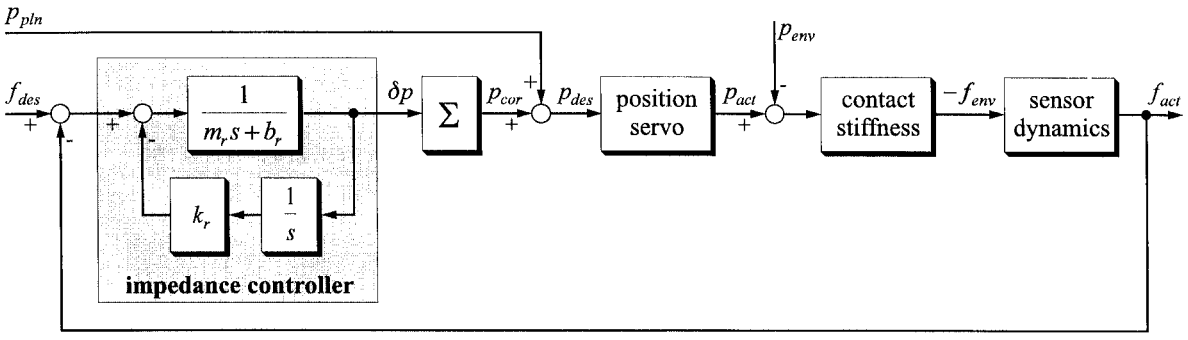

Fig. 12. Impedance control with inner position loop.

https://doi.org/10.1017/S0263574798000162 Published online by Cambridge University Press

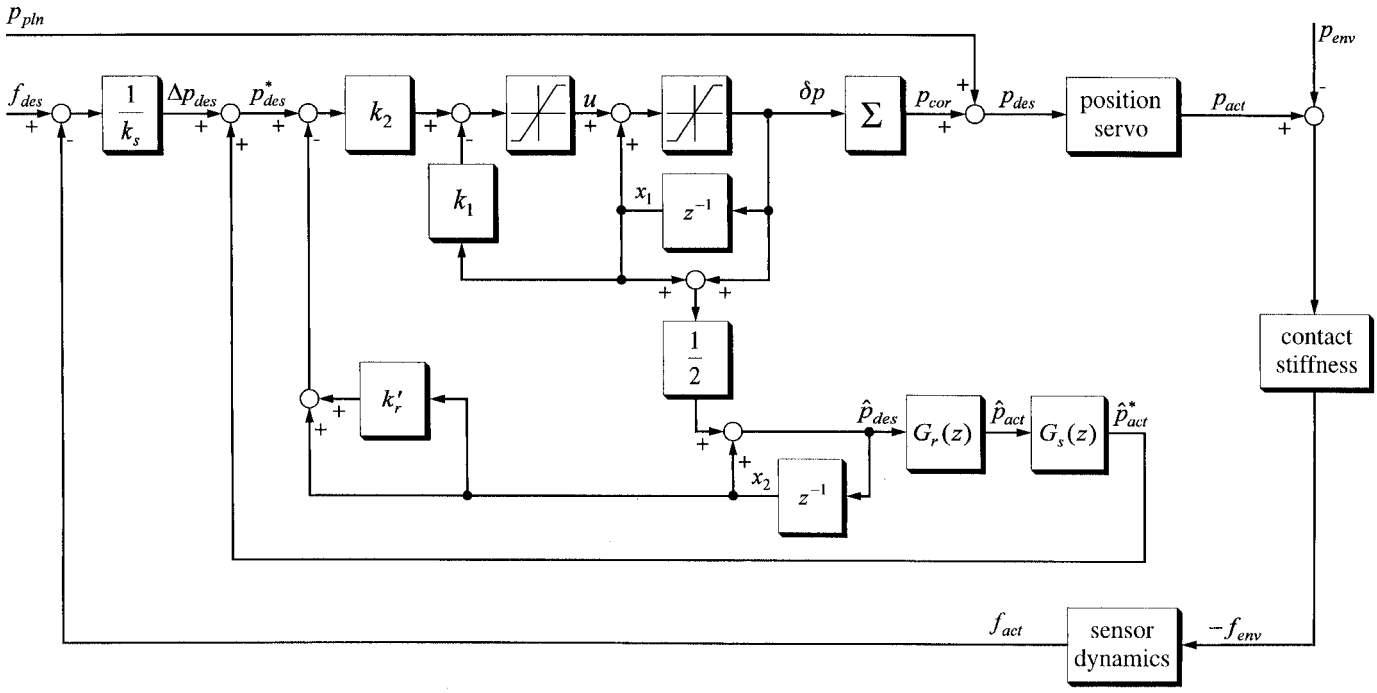

Fig. 13. New controller with the ability of both explicit force control and impedance control.

the desired corrective velocity is zero. Replacing equation (15) and using the structure of Figure 7, a velocity controller with limited acceleration is given by

$$u = \dot{p}^*_{des} - x_1 \tag{26}$$

where $\dot{p}^*_{des}$ is the desired corrective velocity.

The external controller contains some state variables which have to be initialized appropriately. At the beginning of a task-frame control phase, x_1 and x_2 are set to zero and the model of sensor dynamics is initialized so that $\hat{p}^*_{act}$ is zero, too. When switching from one controller to another, e.g. from distance control to explicit force control or from explicit force control to halt control, x_1 and x_2 remain unchanged. If more than one sensor is used, e.g. a force sensor and a distance sensor, models of each are computed permanently. This enables a simple switch to the other model output $\hat{p}^*_{act}$. With this method a perfect switch-over is obtained.

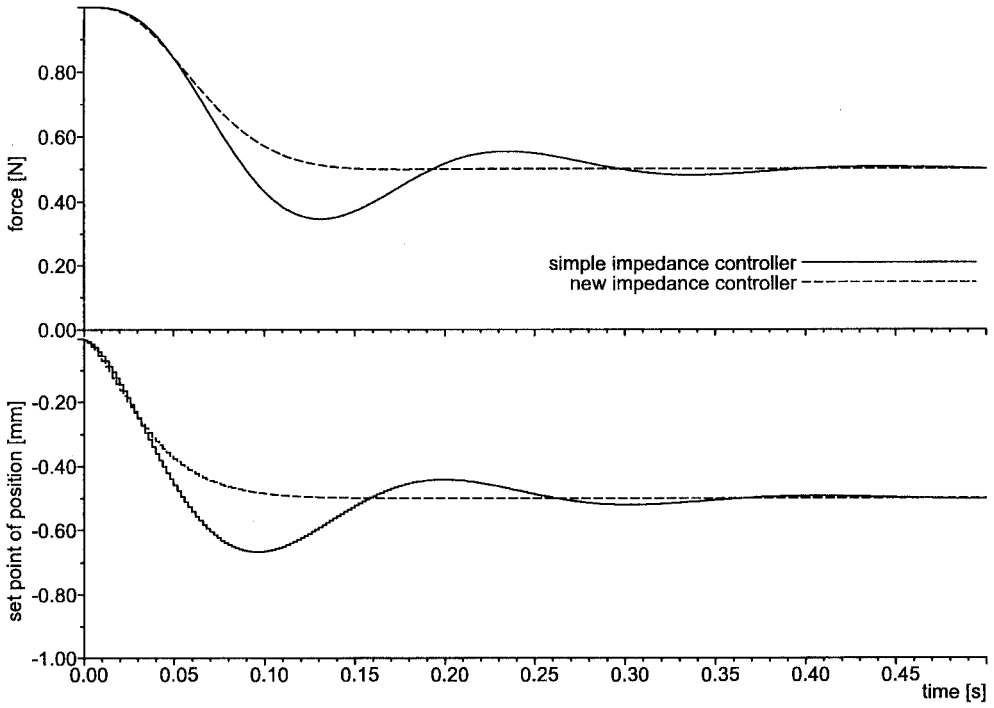

Fig. 14. Response to a step in the environmental position.

https://doi.org/10.1017/S0263574798000162 Published online by Cambridge University Press

Switching to impedance control requires an additional step. The controller of Figure 13 generates an artificial stiffness that pulls the robot back to the planned position. If at switch-over the amount of correction x_2 is non-zero then the robot should be pulled back to this position. To achieve this behavior the current value of x_2 is stored at switch-over and in future subtracted from the actual value prior to the multiplication with k_r'.

10 PRACTICAL RESULTS

The results presented here have been obtained with a *Manutec r2* six-joint industrial robot. Its factory-provided controller has been replaced with a VMEbus-based self-development in order to realize a very fast force control and for other reasons. The joint-based position control loop as well as the superimposed force controller operate at a sample period of 2 ms. A force-torque sensor *SCHUNK FT* 65/5 is mounted in the robot's wrist and connected to the robot controller with a serial line providing measurements at a sample period of approximately 7 ms.

Using the feedback of the position loop error, the force controller's predictor only needs a model of the sensor dynamics and an estimate of the contact stiffness. These can be obtained experimentally with appropriate test movements. Figure 15 shows the recordings of position and force during a position-controlled movement while the robot was in contact with a spring. From the graph of the actual position a fast response in the beginning and a slower one at the end of the movement (where the position error is small) can be observed. This is the effect of the interaction of Coulomb friction with the integral part of the position controller which in section 7 has been stated to be hardly predictable. The comparison of the change in the force measurements with the change of position yields a stiffness constant of $k_s \approx 3.85\,\text{N}/1.7\,\text{mm} \approx 2260\,\text{N/m}$. The sensor dynamics causes the delay of the force measurement to the actual position. The parameters $\tau_s = 10\,\text{ms}$ and $a_s = 120\,\text{s}^{-1}$ for the model given in equation (6) have been identified. The output of the simulated model with the actual position as input is shown in Figure 15, too. The identification was performed by repetitive simulation and manual adaptation of the model parameters to match the measured graph. No complicated identification methods were necessary.

In a second step the force controller was parameterized with these experimentally identified model parameters. A double-pole with $c = 50\,s^{-1}$ and a limitation of acceleration of $a_{\max} = 1\,\text{m/s}^2$ with associated limitation of velocity according to equation (18) were selected. Figure 16 shows a response of this controller to a step in f_{des} with explicit force control. The lower graphs show the actual position and its set point which is smooth as desired. In spite of this smoothness a very fast response without overshoot is achieved.

As test application a robotic grinding facility has been built, wherein the *Manutec r2* is equipped with a grinding tool as sketched in Figure 17. Explicit force control is used to regulate the normal force while moving the tool along the surface. The grinding tool is a wheel with radially mounted abrasive paper. No additional passive compliance is used. The identification of the contact has shown a nonlinear stiffness which is roughly approximated with a stiffness constant $k_s = 12000\,\text{N/m}$. The force controller's low-pass filter is parameterized with $c = 20\,\text{s}^{-1}$ for a lower cut-off frequency in order to filter out high-frequency noise due to mechanical vibrations

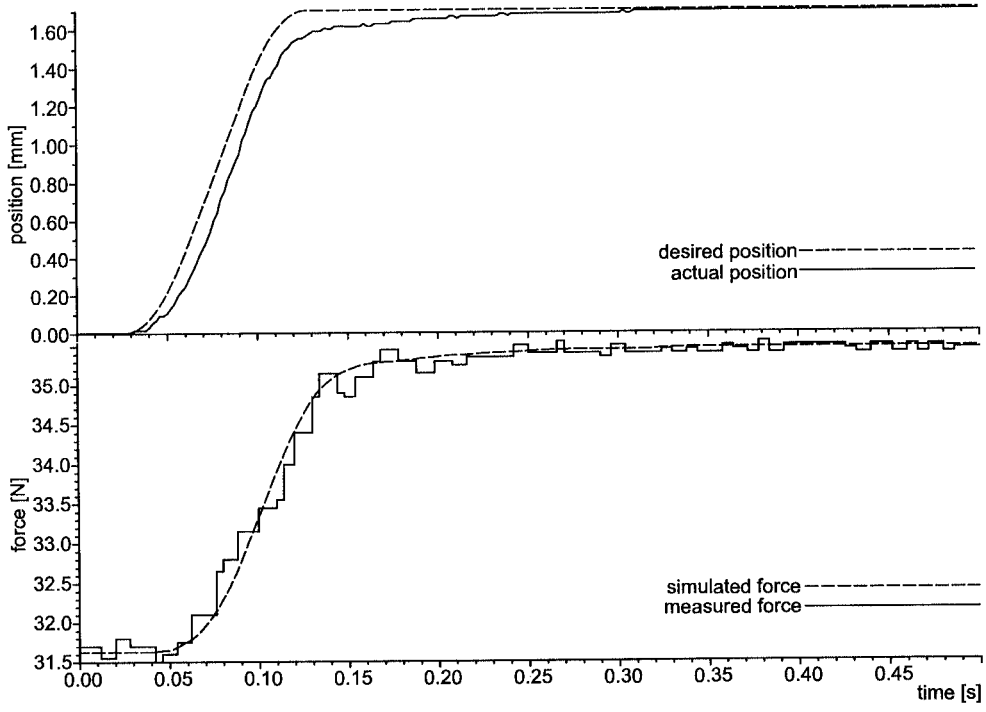

Fig. 15. Position controlled test movement in contact with spring.

https://doi.org/10.1017/S0263574798000162 Published online by Cambridge University Press

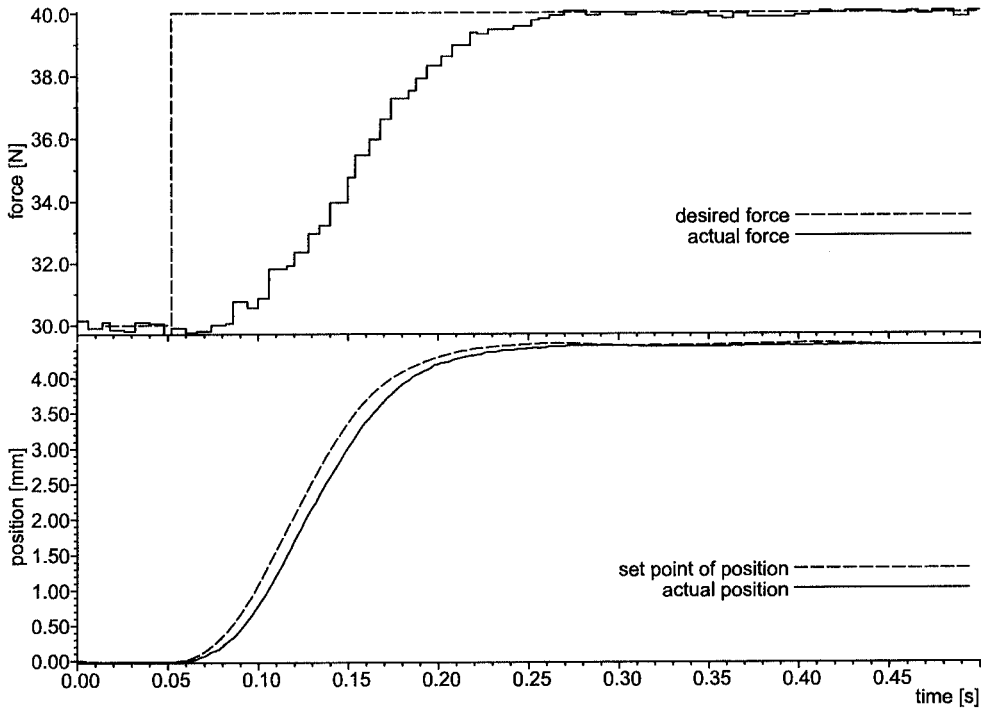

Fig. 16. Step response of force controlled robot in contact with a spring.

resulting from the grinding process. Figure 18 shows recordings of force-controlled grinding. To visualize the control performance, the set point of normal force is switched between 10 and 30 N. Since the force measurements are very noisy, the control performance can better be evaluated from the graph of position which is well smoothened by means of the second-order low-pass filter. The lower cut-off frequency makes the force controller very robust, so that it performs well even under rough conditions including a very imprecisely modeled contact stiffness.

11 CONCLUSION

A new force and impedance control method has been presented. It uses an underlying position feedback loop which is the best way to reject frictional disturbances and has some further advantages with industrial robots. The superimposed force controller generates smooth corrective motions and performs well even with sensors that insert a long dead time into the feedback loop. It is computationally very efficient, easy to understand, and therefore well applicable.

Beyond the experimental data presented in this paper, the force controller has been implemented within a multi-robot control system that is used as testbed for space applications at the Institute of Robotics Research.[18]

The efficiency of force control in practical applications depends on adequate programming methods which are not available with today's robot programming languages. Therefore a new language dedicated to the programming of sensor functions has been integrated into the above mentioned robot control systems and is currently being further developed.

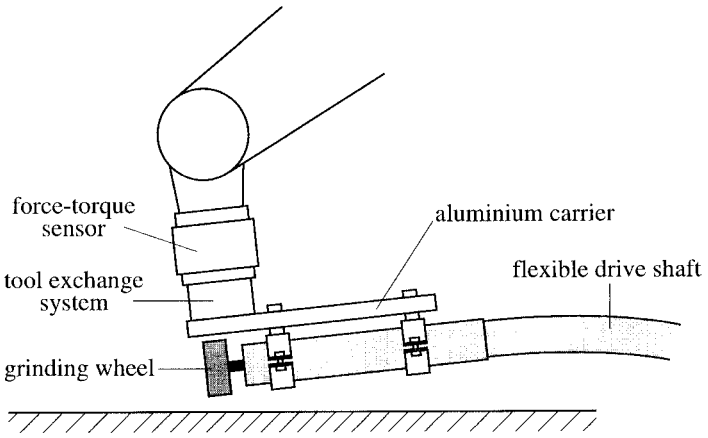

Fig. 17. Configuration of robotic grinding.

https://doi.org/10.1017/S0263574798000162 Published online by Cambridge University Press

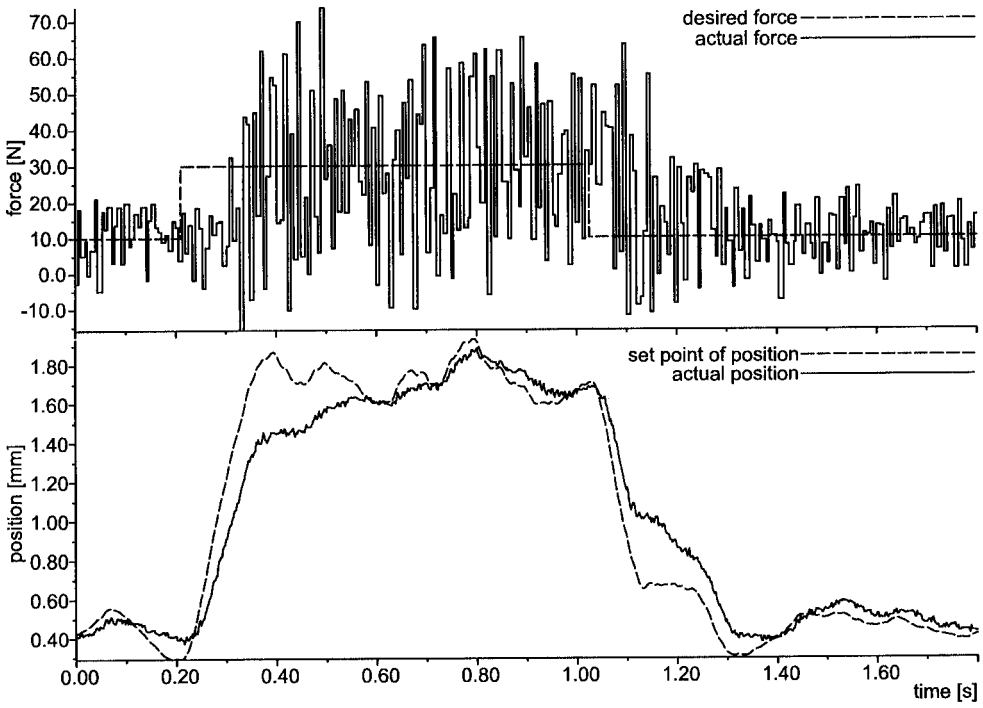

Fig. 18. Step responses of force controlled grinding.

References

1. D.E. Whitney, "Historical Perspective and State of the Art in Robot Force Control" *Int. J. of Robotics Research* **6,** No. 1, 3–13 (1987).
2. M.T. Mason, "Compliance and Force Control for Computer Controlled Manipulators" *IEEE Trans. on Systems, Man, and Cybernetics* **11,** No. 6, 418–432 (1981).
3. M.H. Raibert and J.J. Craig, "Hybrid position/force control of manipulators" *ASME J. of Dynamic Systems, Measurement, and Control* **102,** 126–133 (1981).
4. R.J. Anderson and M.W. Spong, "Hybrid Impedance Control of Robotic Manipulators" *IEEE J. of Robotics and Automation* **4,** No. 5, 288–295 (1988).
5. J.A. Maples and J.J. Becker, "Experiments in Force Control of Robotic Manipulators" *IEEE Int. Conf. on Robotics and Automation* (1986) pp. 695–702.
6. J. De Schutter, "A study of active compliant motion control methods for rigid manipulators based on a generic scheme" *IEEE Int. Conf. on Robotics and Automation* pp. 1060–1065.
7. K.G. Shin and C.P. Lee, "Compliant Control of Robotic Manipulators with resolved acceleration" *IEEE Conf. on Decision and Control* (1985) pp. 350–359.
8. O. Khatib, "A Unified Approach for Motion and Force Control of Robot Manipulators: The Operational Space Formulation" *IEEE J. of Robotics and Automation* **3,** No. 1, 43–53 (1987).
9. G. Hirzinger and K. Landzettel, "Sensory feedback structures for robots with supervised learning" *IEEE Int. Conf. on Robotics and Automation* (1985) pp. 627–635.
10. J. De Schutter and H. Van Brussel, "Compliant Robot Motion II. A Control Approach Based on External Control Loops" *Int. J. of Robotics Research* **7,** No. 4, 18–33 (1988).
11. R. Volpe and P. Khosla, "A Theoretical and Experimental Investigation of Explicit Force Control Strategies for Manipulators" *IEEE Trans. on Automatic Control* **38,** No. 11, 1634–1650 (1993).
12. J. De Schutter, "Improved Force Control Laws for advanced Tracking Applications" *IEEE Int. Conf. on Robotics and Automation* (1988), pp. 1497–1502.
13. R. Colbaugh and K. Glass, "Decentralized adaptive compliance control of robot manipulators" *Robotica* **13** Part 5, 485–498 (1995).
14. J.L. Pei, Q.J. Zhou and T.P. Leung, "A Neural Network Robot Force Controller" *IEEE/RSJ Int. Conf. on Intelligent Robots and Systems (IROS '92)* (1992) pp. 1974–1979.
15. M.C. Fritsch, G. Abba and E. Ostertag, "Fuzzy Force/Position Control for a Robot System" *Fuzzy Duisburg '94: Int. Workshop on Fuzzy Technologies in Automation and Intelligent Systems* (1994) pp. 237–245.
16. O.J.M. Smith, "A Controller to Overcome Dead Time". *ISA J.* **6,** No. 2, 28–33 (1959).
17. D.A. Lawrence, "Impedance Control Stability Properties in Common Implementations" *IEEE Int. Conf. on Robotics and Automation* (1988) pp. 1185–1190.
18. E. Freund and J. Rossmann, "Intelligent Autonomous Robots for Industrial and Space Applications" *IEEE/RSJ Int. Conf. on Intelligent Robots and Systems (IROS '94)* (1994) pp. 1072–1078.

https://doi.org/10.1017/S0263574798000162 Published online by Cambridge University Press